ISSN 0742-0463, Journal of Volcanology and Seismology, 2021, Vol. 15, No. 6, pp. 414–434. © Pleiades Publishing, Ltd., 2021.
Russian Text © The Author(s), 2021, published in Vulkanologiya i Seismologiya, 2021, No. 6, pp. 59–80.

Crustal Seismotectonic Deformations in Central and Western Tien-Shan

N. A. Sycheva*

Research Station, Russian Academy of Sciences in Bishkek city, Bishkek-49, 720049 Kyrgyzstan

**e-mail: ivtran@mail.ru*

Received December 4, 2020; revised March 30, 2021; accepted August 26, 2021

Abstract—This study is concerned with Western and Central Tien-Shan. It is an area of intracontinental collision and is of great interest for the study of the geodynamic processes that are occurring in the crust. The area of study was investigated using the method of seismotectonic deformation (STD). The STD was calculated on the basis of the approaches proposed by Yu.V. Riznichenko and S.L. Yunga. We used the ISC (International Seismological Centre, London) catalog for estimating the seismicity distribution, for calculating the mean annual rate of STD (STD intensity) I_Σ, and the parameter of concentration of earthquake-generating ruptures K_{CP}. The catalog includes over 84000 earthquakes for the period 1902–2019. The distribution of the parameters mentioned above was calculated for three depth ranges: 0–5, 5–25, and over 25 km. We identified areas of intensive seismotectonic deformation, seismic activity, and high concentration of earthquake-generating faults. The study of the entire earthquake-generating layer gave the result that the maximum STD intensity $I_\Sigma = \sim 9 \times 10^{-8}$ yr^{-1} was obtained for the junction zone between Southern Tien-Shan and Northern Pamirs. As to the north part of the area of study, high values of STD intensity were obtained for the western Terskey Alatau: $I_\Sigma = \sim 2 \times 10^{-9}$ yr^{-1}. At all the depths studied here, the maximum rate of earthquakes occurs in the Gissar-Kokshaal earthquake-generating zone. In the northern part, high seismicity is characteristic for the mountain ranges that encircle the Issyk Kul Basin (Terskey Alatau, Kungei Alatau, and Zailiisky Range). The area of study typically exhibits a high level of the concentration of earthquake-generating ruptures, with most of these lying at depths of 0–5 km. Our study of STD directivity is based on data for focal mechanisms of 11376 earthquakes occurring in 1949–2020. We plotted diagrams showing the distribution of azimuthal directions for the principal stress axes. The azimuth of the compression axis for most events falls within the sector 300°–360°. The resulting STD maps were inspected to determine the directions of shortening and lengthening axes, and to note that the deformation settings show a great diversity in the area of study. The STD tensors obtained for the depths 5–25 km (the earthquake-generating layer) were used to find the distributions of the Lode–Nadai coefficient μ_ε, of the sum of the horizontal components (XX + YY), and of the vertical component (ZZ). We determined areas that show simple compression and maximum shortening. The models of crustal deformation derived by the STD method and from GPS data were compared to find a fairly good consistency.

Key words: earthquake, focal mechanism, tensor of seismotectonic strain rate, principal stress axes, axes of shortening and lengthening, Lode–Nadai parameter, vertical component of STD rate tensor

DOI: 10.1134/S0742046321060105

INTRODUCTION

The area of study is a complex-structured, long-evolving fold-and-block mountain edifice. It contains parts of two different major geotectonic areas, viz., an epi-Paleozoic platform and an Alpine geosyncline. The Tien Shan mountain country was created during the endogenous activation of the epi-Paleozoic platform starting at the end of the Oligocene, at the same time with the terminal phase of the closing of the Alpine geosyncline. The main present-day features of Tien Shan were formed during Quaternary time. The activation process was occurring nonuniformly over time and in space. As an example, a quiescence in movements is noted in the Late Pliocene and in the Early Pleistocene, to give way to a new impulse of tectonic activity. The impulse has been continuing until now. This is indicated by the presence of intensive recent movements whose amplitudes reach considerable values, as well as by high seismic activity.

Tien Shan extends for about three thousand kilometers from 65° to 95° E, its broadest part is on the order of 400 km wide. Tien Shan is subdivided into the Western, the Central, the Eastern, and the Dzhungar geologic–geographic provinces. The Western Tien Shan lies west of the Talas–Fergana fault. The Central Tien Shan is between the Talas–Fergana fault in the west and the 80° longitude in the east. The Eastern Tien Shan extends from the 80° longitude in the west

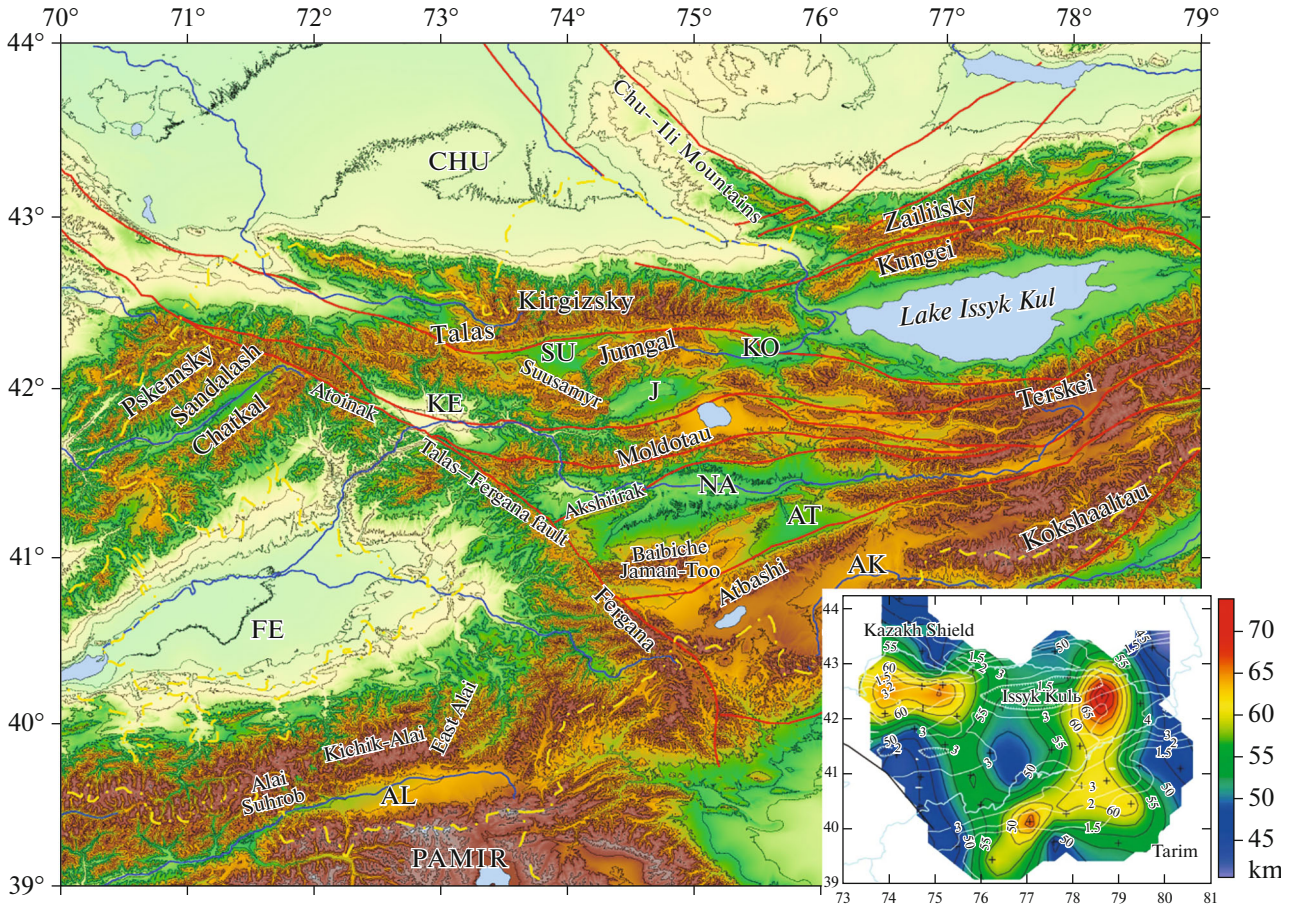

Fig. 1. Mountain ranges, valleys, and rivers in Western and Central Tien Shan. Intermontane and piedmont basins: AL Alai, AK Aksai, AT Atbash, J Jumgal, KE Ketmen–Tyube, KO Kochkor,NA Naryn, SU Suusamyr, CHU Chu (after Burtman (2012)). The yellow dashed line marks the Kirghizian border. Red lines represent regional faults after Chediya (1986). The insets shows the depths to the Moho (after Vinnik et al. (2004)). White lines shows smoothed topographic contours.

to the Jungar (Borohoro) fault in the east. Northeast of the Jungar fault lies the Jungar Tien Shan. The Western and Central Tien Shan mostly lie within the area of Kirgizia. Tien Shan is bounded by the Turanian plate to the north, to the south it is bounded by the Tarim Basin in the east and by the Tajik Depression in the west, which are connected by the Alai valley and the Surhob R. valley.

The region contains many faults that have been active during Late Quaternary time. The Cenozoic folds and faults in Tien Shan are described in numerous publications (Makarov, 1977; Sadybakasov, 1990; *Sovremennaya geodinamika ...,* 2005; Trifonov et al., 2002; Trofimov et al., 1976; Chediya, 1986; Shults, 1948, among others).

The present-day bottom of intermontane basins in Tien Shan (except for the Turfan Basin) lies above sea level and above the adjacent parts of the Kazakhstan Platform. The top of the Paleozoic basement is above sea level in small intermontane basins, while being below sea level in the axial parts of large basins (the Fergana, Alai, Afghan–Tajik, Aksai, Atbash, Naryn, Issyk-Kul, Jumgal, Talas, Chu, and Turfan basins). The basement in the Issyk-Kul and the Naryn basins lies at a depth greater than 3 km, the figure being about 2 km in the Chu Basin and up to 9 km in the Fergana Basin (Fig. 1) (Burtman, 2012).

According to Vinnik (2004), there are two distinct strips of thicker (more than 55 km) crust within Tien Shan separated by an area of shallow Moho (see Fig. 1, inset). The northern strip coincides with the uplifts of the Kirgizsky, Zailiisky Alatau, and Kungei Alatau mountain ranges (see Fig. 1), while the southern strip is that of the uplifts of the Gissar–Alai mountain range system. Apart from these strips which strike in the Tien Shan direction, there are several transverse structural elements. As an example, the Lake Issyk Kul area contains a nearly north–south striking area of thicker crust extending southwards (see Fig. 1, inset).

The Tien Shan epi-platform orogeny is nearly all of it in a zone of VIII–IX intensity seismicity. On the west and north it is bounded by a strip where the seismic effect does not exceed intensity VII. Most epicenters of large ($M = 5$) earthquakes extend as two earth-

Table 1. Parameters of several large earthquakes in Tien Shan (after Mamyrov et al. (2002))

No.	Date	φ°, N	λ°, E	*H*, km	*M*	Designation
1	1475	42.6	75.2	15	6.4	Balasagun
2	1716	41.2	80.3	30	7.5	Aksui
3	1770	42.8	74.1	15	6.0	Belovodsk
4	1807	43.1	76.9	20	6.7	Alma-Ata
5	22 Mar. 1865	42.7	73.2	15	6.4	Merken
6	2 Aug. 1885	42.7	74.1	15	6.9	Belovodsk
7	8 Jun. 1887	43.1	76.8	20	7.3	Vernyi
8	11 Jul. 1889	43.2	78.7	40	8.3	Chilik
9	22 Aug. 1902	39.8	76.2	40	8.1	Kashgar
10	3 Jan. 1911	42.9	76.9	25	8.2	Kemin
11	29 Feb. 1916	40.6	78.2	20	5.8	Kokshaal
12	20 Jun. 1938	42.7	75.8	21	6.9	Kemin-Chu
13	20 Apr. 1941	39.2	70.5	15.6	6.4	Garm
14	2 Oct. 1946	41.9	72.0	30	7.5	Chatkal
15	28 Jan. 1948	41.4	75.3	6	4.9	Kulanak
16	10 Jul. 1949	39.2	70.8	16	7.4	Khait
17	5 Jun. 1970	42.5	78.9	15	6.8	Sarykamysh
18	24 Mar. 1978	42.9	78.7	30	6.8	Zhalanash-Tyupe
19	26 Oct. 1984	39.3	71.3	15	6.4	Jirgatal
20	23 Aug. 1985	39.4	75.4	20	7.0	Kashgar
21	12 Nov. 1990	42.9	78.0	20	6.4	Baisorun
22	19 Aug. 1992	42.1	73.6	25	7.3	Suusamyr

quake-generating zones, the North Tien Shan zone and the Gissar–Kokshaal (South Tien Shan) zone, which tend, respectively, to the northern and southern parts where the orogen has a contrasting boundary, and which bound it by the Turanian plate and the Kazakh Shield to the north and by the Tarim Platform to the south. The Gissar–Kokshaal zone shows high seismicity in the junction between the Pamirs and Tien Shan (Fig. 2a).

These two zones, which are seismic sutures of the first category, serve as boundaries between major blocks, Turan–Tien-Shan–Tarim. These seismic sutures can generate earthquake magnitudes that are the greatest possible for the crust, $M > 8$ (Yudakhin and Chediya, 1991). In Fig. 2A we use stars to mark the locations of large earthquakes with $M \geq 5$ in Tien Shan, see Table 1 which contains a catalog of large historical earthquakes. The highest density of earthquakes occurs both in the Southern Tien-Shan zone and in the Northern Tien-Shan zone. One can see in this figure that the bulk of large earthquakes makes a strip that includes the northern wall of the Kirgizsky mountain range and the uplift system of the Zailiisky Alatau and Kungei Alatau. Very strong earthquakes have occurred there such as the Belovodsk, Vernyi, Chikik, Kemin, and Kemin-Chu events (see Table 1). The grandest paleo seismic ruptures and $M > 8$ earthquakes are known to have occurred in the Kungei area, while west and east of it the seismic activity is lower, with the maximum occurring in the internal part of the area.

The geodynamic processes in the area of study as inferred from seismic data were previously studied by Yunga (1990), Trifonov et al. (2002), Kuchai and Bushenkova (2009), Rebetsky and Alekseev (2014), among others. The data analysis in these works was based on the STD method (Riznichenko, 1985; Yunga, 1990) or on the method of cataclastic analysis (MCA) as applied to tectonic discontinuities (Rebetsky, 2007), or else researchers considered the focal mechanisms of moderate and large earthquakes (Kuchai and Bushenkova, 2009). In (Yunga, 1990; Rebetsky and Alekseev, 2014; Kuchai and Bushenkova, 2009), and their area of study is much larger than that considered in the present paper. Trifonov et al. (2002) made a detailed study of STD fields in an area that includes the geological structures of Southern Tien Shan, the Afghan–Tajik Depression, the Pamirs, and North Hindu Kush.

We at the Research Station of the Russian Academy of Sciences (SS RAS) studied the state of stress and strain in the crust of Northern and Central Tien Shan using two methods, STD and MCA. The results were

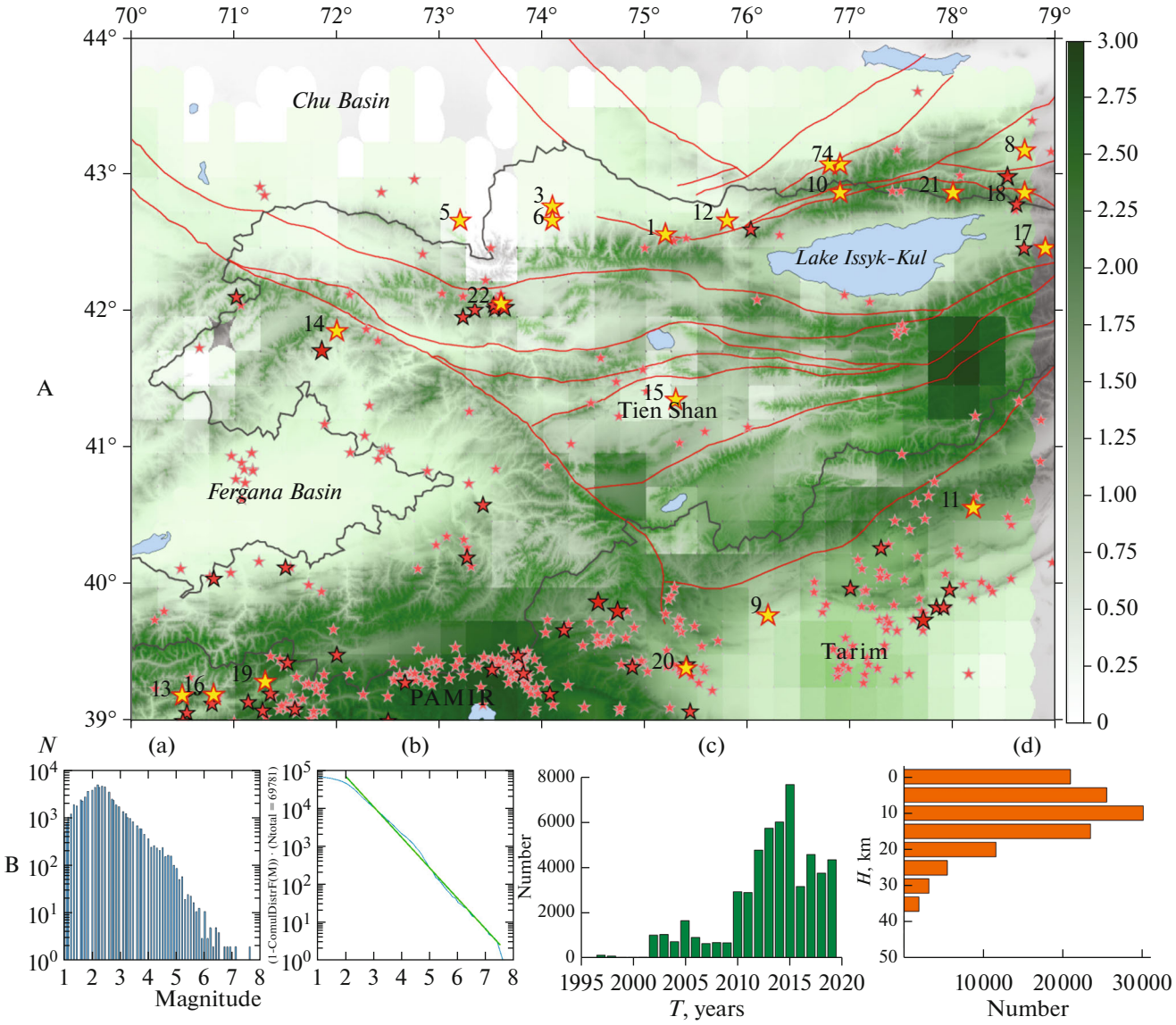

Fig. 2. A quantitative distribution of earthquakes from the ISC catalog, with stars marking earthquake epicenters: pale pink is for $5 \le M < 6$, pink for $6 \le M < 7$, red for $M \ge 7$, yellow for historical earthquakes, with earthquake identification numbers being the same as in Table 1. Red lines represent regional faults, the grey line marks the Kirghizian border (A); the distribution of some characteristics from the ISC catalog; (a) over magnitude, (b) cumulative Gutenberg–Richter distribution, (c) over time, (d) over depth (B).

reported in (Sycheva et al., 2005a, 2008; Sycheva and Mansurov, 2016, 2017; Rebetsky et al., 2012, 2016). The accumulation of data on earthquake focal mechanisms allows one to expand the area of study and to refine the results.

Recent movements in the region under study are extensively investigated using GPS technologies. These studies are based on data supplied by the Central Asian (CA) GPS network (the observation sites are both inside and around the region under study). There are well-known works on this area of research (Abdrakhmatov et al., 2001; Reigber et al., 2001; Midi et al., 2001; Zubovich et al., 2001, 2004, 2010; Kostyuk et al., 2010; Zubovich and Mukhamediev, 2010; Kuzikov and Mukhamediev, 2010; Mansurov, 2017, among others). These works report results in the development of strain models for the crust of Tien Shan based on GPS observations.

The presence of several works in the estimation of stress and strain based on seismic and GPS observations indicates a great interest in this area. It would not appear to be a gross exaggeration to say that comparison of crustal seismotectonic deformations with GPS observations is also of considerable interest.

The goal of the present study is to estimate the state of stress and strain in the crust of Western and Central

Tien Shan based on data of seismicity and focal mechanisms of earthquakes using the STD method, to present the results using modern approaches to mapping, as well as to compare them with models for the distribution of crustal deformations obtained previously from GPS observations.

THE METHOD

We used the STD method to estimate the state of stress and strain in the area of study. The method is described in many publications (Lukk and Yunga, 1979; Riznichenko, 1985; Yunga, 1990, among others) and remains in use today (Lukk et al., 2015; Sycheva and Mansurov, 2017; Lukk and Shevchenko, 2019, among others). Considering all earthquakes that have occurred in an earth volume V for a time T, the resulting averaged inelastic deformation due to these events can be described by a tensor of the rate of rupture (seismotectonic deformation) $\langle \varepsilon_{ij} \rangle$ (Yunga, 1990; Riznichenko, 1985):

$$\langle \varepsilon_{ij} \rangle = \frac{1}{\mu VT} \sum_{\alpha=1}^{N} M_0^{(\alpha)} m_{ij}^{(\alpha)}, \quad (1)$$

with the summation being over seismic events indexed by α; N is the number of events. In (1), $M_0^{(\alpha)}$ is the seismic moment of the earthquake indexed $^{(\alpha)}$, $m_{ij}^{(\alpha)}$ is the direction tensor of the mechanism, μ is the shear modulus, V is the earth volume studied, and T is the time of study. When the period of time is in years, the tensor $\langle \varepsilon_{ij} \rangle$ is also referred to as the annual increment of seismotectonic deformation. Yunga (1990) and Lukk and Yunga (1979) proposed approximating (1) by the following expression:

$$\langle \varepsilon_{ij} \rangle = \frac{1}{\mu VT} \sum_{\alpha=1}^{N} M_0^{(\alpha)} \sum_{\alpha=1}^{N} m_{ij}^{\alpha} = I_\Sigma \sum_{\alpha=1}^{N} m_{ij}^{\alpha}, \quad (2)$$

where a scalar characteristic is introduced giving the increment of seismotectonic deformation I_Σ, which is referred to as STD intensity.

With a view to calculating the directivity of seismotectonic deformation by averaging the initial data, we divided the geostructural area into elementary subareas with a radius which are centered at grid points of a selected grid. The STD is calculated by summing the matrices of individual mechanisms within each elementary subarea. The grid points are chosen in a grid at intervals of 0.2° (~20 km) having the radius of an elementary subarea equal to $r = 0.5°$ (~50 km), which provides for data smoothing. An area of $r = 0.5°$ can also be the potential zone where a large earthquake would occur (its diameter is 100 km). The STD intensity is found by summing scalar seismic moments within each area along the lines of (Lukk and Yunga, 1979). For constructing a map of averaged focal mechanisms, we chose the grid points on a grid at intervals of 0.5° (~50 km) and the radius of an elementary area equal to $r = 0.5°$. The STD is mapped using a classification of seismotectonic deformation regimes based on parameterization of the regimes via a system of angular parameters to provide for an isometric representation of tensor objects onto a sphere (Yunga, 1990, 1997).

The concentration of earthquake-generating ruptures parameter C_{EGR} has a clear physical meaning, being the ratio of the mean distance between earthquake-generating ruptures that have occurred in a seismic earth volume V_0 for a time ΔT, to the mean length of the ruptures (Sobolev and Zavialov, 1980; Zavialov, 2006):

$$C_{EGR} = \eta^{-1/3} / l_{mean}, \quad (3)$$

where $\eta = N/V_0$ is the volumetric density (concentration) of ruptures based on past earthquakes; $l_{mean} = \frac{1}{N} \sum_j l_j$ is the mean rupture length in an ensemble of cracks; N is the total number of earthquakes in the energy class range $[K_{min}, K_{max}]$ that have occurred in an elementary seismic volume V_0 for a time ΔT; l_j is the length of an individual earthquake-generating rupture to be found from the relation

$$\log l_j = aK_j + c, \quad (4)$$

where K_j is the energy class (or magnitude) of an earthquake. Different seismic regions may have different values of the constants a and c.

The experience in using C_{EGR} in several seismic regions worldwide shows that the best choice of the constants is (Riznichenko, 1976): $a = 0.244$, $c = -2.266$. When using magnitude instead of energy class, one should replace K_j with M in (4), but the constants would then have the following values: $a = 0.440$, $c = -1.289$.

The STD intensity, the number of earthquakes, and the concentration of earthquake-generating ruptures were found for each $0.2 \times 0.2°$ grid element in the area of study. The step was 0.1°.

THE DATA SET

The earthquake catalog. We determined the spatial location of seismicity (vertical cross sections), analyzed seismic activity (the number of earthquakes per unit area), and estimated STD intensity using the ISC catalog (*International ...,* 2019), which contains over 84000 earthquakes that have occurred in 1902–2019 in the area of study (see Fig. 2A). Some characteristics of this catalog are shown in Fig. 2B and listed in Table 2. Magnitudes are assigned to 69781 earthquakes, with ~86% of all events having their energy characteristics based on body waves (M_b), while depths are known for 71284 events.

The bulk of the ICS catalog consists of $2 \le M \le 6$ events (see Fig. 2B(a)), which mostly occurred after

Table 2. Characteristics of the ISC catalog

Initial date	End date	N	φ_1°, N	φ_2°, N	λ_1°, E	λ_2°, E
1	2	3	4	5	6	7
22 Aug 1902	30 Dec 2019	84857	39°00′	44°00′	70°00′	79°00'
Quantitative characteristic	Magnitude					Depth
	M_b	M_L	M_{pv}	M_S	None	
	8	9	10	11	12	13
N	60052	3254	6428	69	69	68198
%	86	4.8	9	0.1	0.1	80

Table 3. Characteristics of catalogs of focal mechanisms

Source of catalog	Period	N	φ°, N	λ°, E	M
RS RAS (PFM)	24 Sep. 1994 to 29 Dec. 2018	1577	42.00–43.00	73.75–76.00	1.06 – 5.4
RS RAS (WIM)	14 Jan. 1996 to 30 May 2020	320	40.50–43.66	72.00–77.99	2.81–5.70
KIS1	2 Nov. 1946 to 24 Dec. 1994	5467	38.26–43.98	68.30–81.00	0.50–7.20
KIS2	4 Jan. 1994 to 28 Dec. 2005	684	39.00–43.43	69.15–80.67	3.11–6.11
SOME MON RK	2 Jan. 1996 to 31 Dec. 2002	3445	40.42–48.57	67.08–84.62	0.11–5.67
CMT catalog	28 Jul. 1976 to 27 Oct. 2019	185	39.00–43.72	70.02–78.98	4.70–7.20

SS RAS stands for Research Station of the Russian Academy of Sciences, PFM stands for based on *P* first motions, VIM stands for wave inversion method, KIS denotes the Institute of Seismology, National Academy of Sciences, Kyrgyz Republic; SOME MON RK, Almaty means Seismological Technique Testing Expedition of the Ministry of Education and Science, Republic of Kazakhstan, CMT stands for *Centroid moment tensor* (*Search form* ..., 2020).

2002 (see Fig. 2B(b)) at depths of 0–25 km (see Fig. 2B(e)). According to the Gutenberg–Richter plot (see Fig. 2B(c)), the part of the catalog reported completely includes $3 \le M \le 7.5$ events.

The catalog of focal mechanisms. We based our STD calculations on several data sources relating to earthquake focal mechanisms. Along with the catalogs of focal mechanisms obtained at the SS RAS, we also analyzed catalogs compiled by other organizations. Some of these data were in part used and described in (Sycheva et al., 2005, 2005a, 2008; Kalmetieva et al., 2010; Sycheva and Mansurov, 2017; Sycheva, 2020). Some characteristics of the data sources are presented in Table 3.

Most events in the combined catalog of focal mechanisms (FM, 11376 earthquakes) are low magnitude earthquakes ($1.5 \le M \le 3.5$, Fig. 3A(a)). The earthquakes are not uniform over time, with the more completely reported periods being those from 1978 to 1991 and from 1996 to 2001 (see Fig. 3A(b)). The bulk of the events occurred at depths of 0–25 km (see Fig. 3A(c)).

The epicenter location and mechanism type from the FM catalog are shown in Fig. 3B. The color indicates the data source (see the caption to Fig. 3). The radius of a source model represents the earthquake magnitude.

There is a variety of earthquake mechanisms in the area of study (see Fig. 3B). Krestnikov et al. (1987) in their study of Northern and Central Tien Shan based on geological and seismic data noted a great diversity of earthquake mechanisms in the region as a whole, but three mechanism varieties are dominant. The first of these has its compression axis horizontal and looking northeast, while the tension axis is nearly vertical; this type of source is characterized by reverse faulting combined with equally likely rupture planes striking nearly east–west and nearly north–south. The field in the second type has the tension axis horizontal and looking northeast, while the compression axis dips steeply southeast, which provides evidence of a normal-oblique character of movement with equally likely rupture planes that are oriented as in the first case. The third type of mechanism has both of the axes nearly horizontal, but the compression axis strikes northwest, while the tension axis looks northeast, indicating strike slip movements. The planes of equally likely ruptures are oriented as at the sources of the first two. Now the most general mechanism of earthquake source indicating the most general features in the present-day regional stress field has its compression axis oriented northwest, while the tension axis is nearly vertical during reverse movements at the source. The planes of equally likely ruptures are again oriented nearly north–south and nearly east–west.

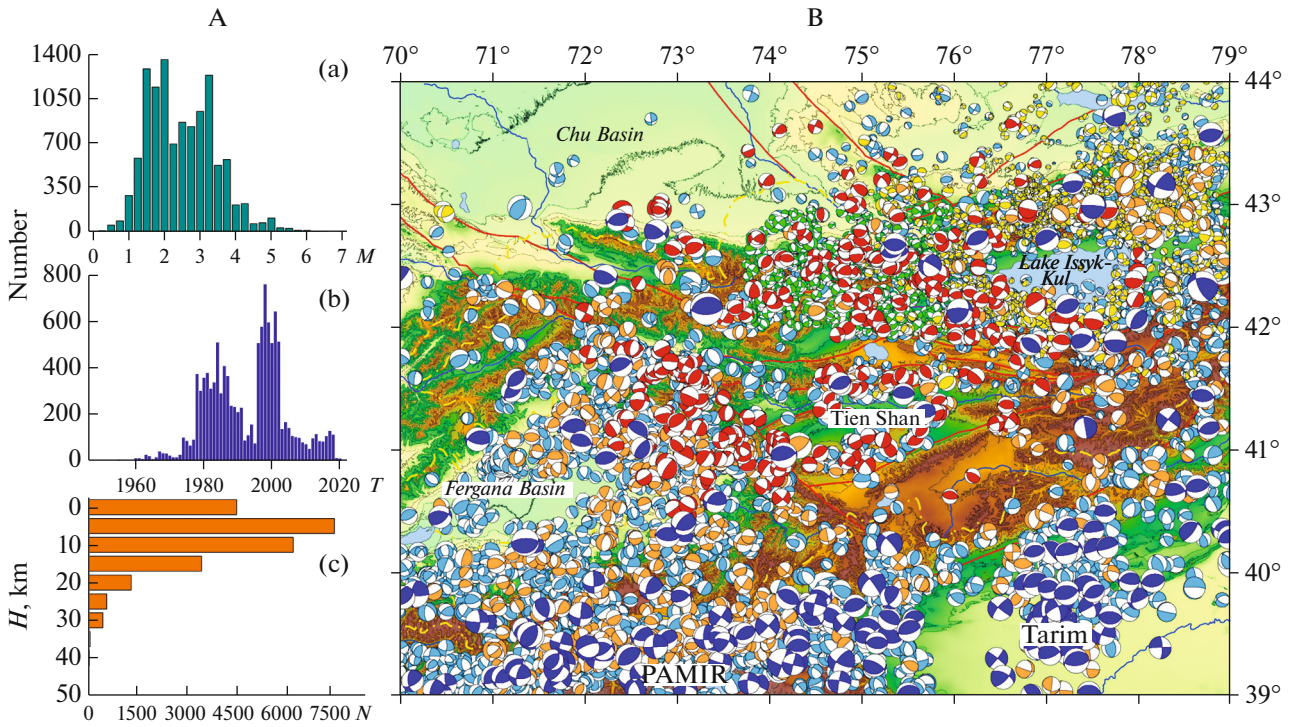

Fig. 3. The distribution of some characteristics in the catalog of focal mechanisms (FM) over magnitude (a), over time (b), and over depth (c) (A); Epicenters and focal mechanisms of earthquakes. The color of a mechanism symbol indicates the data source: light blue (2422 events) denotes the Institute of Seismology, NAN KR and other sources, 1949–1994; orange (380) indicates the Institute of Seismology, NAN KR, 1994–2005; dark blue (185) indicates the CMT catalog for 1976–2019; green indicates RS RAS (based on *P* first motion data), 1994–2018; red indicates RS RAS (the method of wave inversion), 1996–2020; yellow indicates SOME MON RK, Almaty, 1996–2002. Red lines represent regional faults (B).

THE RESULTS

A qualitative Distribution of Seismicity

Our analysis of the seismicity distribution and STD intensity as functions of depth was based only on those earthquakes from the ISC catalog which had depth of focus and magnitude assigned (56766 events).

The distribution of seismicity over depth based on the ISC and FM catalogs is shown in integral projections onto the vertical plane. Two cross sections are in the east–west direction and three for north–south. For the east–west direction each area includes 2.5° of latitude and 9° of longitude. For the north–south direction, each area includes 3° of longitude and 5° of latitude. In the integral projections, the earthquake locations from the ISC catalog are marked black and those from the FM catalog are red.

These constructions revealed the fact that earthquakes occur at depths of 0–50 km in the area of study. The lower boundary in the north of the area of study (Fig. 4A(a)) is at a depth of ~35 km (according to Yudakhin (1983), earthquakes occur down to 30 km depth); in the southern part (see Fig. 4A(b)), the lower boundary of seismicity is deeper, 40 km, with some earthquakes even occurring as deep as 50 km or more. Three layers of seismic activity are identified in all the cross sections considered: the first layer includes events with depths between 0 and 5 km (the shallow layer), the second from 5 to 25 km (the active earthquake-generating layer), and the third layer is deeper than 25 km. The bulk of the events are concentrated in the Northern Tien Shan earthquake-generating zone (28958 events, see Fig. 4A(a)) and in the Southern Tien Shan zone (27808 events, see Fig. 4A(b)) as noted in the Introduction. The integral projections also showed that the seismicity is concentrated in well-defined vertical structures (see Fig. 4B), which may correspond to the depths of the responsible faults. If we subdivide the area of study into the western, the eastern, and the central part, we can see that the greater part of earthquakes occurred in the central part which includes the Kirgizsky mountain range, an area along the Talas–Fergana fault, and the junction zone between the Southern Tien Shan and the Northern Pamirs (see Fig. 4B(b)).

The Areal Distribution of STD Intensity and Seismicity Rate

In consideration of the abovementioned distribution of seismicity over depth (see Fig. 4), we calculated STD intensity I_Σ and seismic activity (the numbers of

Table 4. Grid-element coordinates, minimum and maximum STD intensity I_Σ, and geographic designation for different depths of investigation

H, km	Coordinates		Location	I_Σ, $\times 10^{-9}$ year^{-1}	
	λ, ° E	φ, ° N			
0–50	73.63	43.38	Chu Basin	min	0.0003
	73.88	39.13	Central part of junction zone between Tien Shan and Pamirs	max	94.2
0–5	73.38	42.38	Western Kirgizsky mountain range	min	0.0005
	73.88	39.13	Central part of junction zone between Tien Shan and Pamirs	max	200.3
5–25	70.63	40.88	Northwest side of Fergana Basin	min	0.0004
	73.88	39.13	Central part of junction zone between Tien Shan and Pamirs	max	225.1
25–50	70.63	40.88	Northwest side of Fergana Basin	min	0.0004
	73.63	39.38	Central part of junction zone between Tien Shan and Pamirs	max	25.2

H is depth, λ longitude; φ is latitude; I_Σ is STD intensity.

earthquakes in grid elements) both for the entire seismic layer 0–50 km and for the three depth ranges 0–5, 5–25, and greater than 25 km. Our calculation of these parameters was based on those earthquakes in the ISC catalog which have occurred between 1997 and 2019 (this is the period that is reported with the highest completeness, the rate is over 300 earthquakes per annum, see Fig. 2B(c)). No earthquakes larger than magnitude 6 have occurred in the Northern Tien Shan earthquake-generating zone during the period of interest. The last significant earthquake, the Suusamyr event of August 19, 1992, $M = 7.3$, took place before that period.

The minimum and maximum values of STD intensity, as well as the relevant areas for each of the depth layers, are listed in Table 4.

The areal distribution of the above characteristics at different depths is shown in Fig. 5: on the left is the logarithm of STD intensity, on the right is the logarithm of the number of earthquakes. All the depth layers show maximum STD intensity for the junction zone between the Southern Tien Shan and the Northern Pamirs (~9×10^{-8} yr^{-1}). The lowest STD rate occurs in the Chu valley, in the western Kirgizsky mountain range, and in the northwestern sides of the Fergana Basin (~3×10^{-13} yr^{-1}). The maximum seismicity rate is also observed in the zone where the Southern Tien Shan is adjacent to the Northern Pamirs and Tarim.

The STD intensity is an order higher at depths of 0–5 km than that for the entire earthquake-generating layer, being 2×10^{-8} yr^{-1}. The maximum seismicity at that depth occurred in the area of the Ak-Shyirak mountain range situated south of the eastern Terskei Alatau mountain range.

In addition to the junction zone between the Southern Tien Shan and the Northern Pamirs mentioned above, one notices at depths of 5–25 km several areas with high values of STD intensity. The Northern Tien Shan earthquake-generating zone has two areas in Terskei Alatau where the level of STD intensity reaches ~2×10^{-9} yr^{-1} and ~6×10^{-9} yr^{-1}. At the Alai mountain range, the level of STD intensity varies between 4×10^{-9} yr^{-1} and 5.6×10^{-9} yr^{-1}, while being 4×10^{-9} yr^{-1} at latitude 41° N in the Talas–Fergana fault zone. At that depth considerable numbers of earthquakes occur in the junction zone between the Southern Tien Shan and the Northern Pamirs, as well as in the sides of the Issyk Kul Basin (Kungei, Terskei Alatau, Zailiisky mountain range) and at the Alai mountain range.

Intensive deformation still occurs at depths over 25 km in the junction zone between the Southern Tien Shan and the Northern Pamirs (2.5×10^{-8} yr^{-1}), with the maximum seismicity being observed there as well.

The Concentration of Earthquake-Generating Ruptures Parameter

Sobolev and Zavialov (1980) and Zavialov (2006) used the parameter in earthquake prediction. The present study uses the parameter, because it can reflect the two preceding characteristics together, since the calculation of the parameter is based both on the number of earthquakes occurring in an earth volume and on earthquake class (or magnitude). Figure 6 shows the distribution of the concentration of earthquake-generating ruptures for all the depths concerned. Blue marks low values of the parameter (see Fig. 6), indicating a high concentration of cracks.

High levels of crack concentration at depths of 0–5 km is typical of the entire zone where the Southern Tien Shan is adjacent to the Northern Pamirs and Tarim, of the sides of the Issyk Kul Basin (Terskei and Kungei Alatau, Zailiisky mountain range), of the eastern Kirgizsky mountain range, of the south sides of the Fergana Basin (the Alai mountain range), and of the area along the Talas–Fergana fault. High levels of crack concentration occur in the same areas at depths of 5–25 km as at depths of 0–5 km, but the areas are

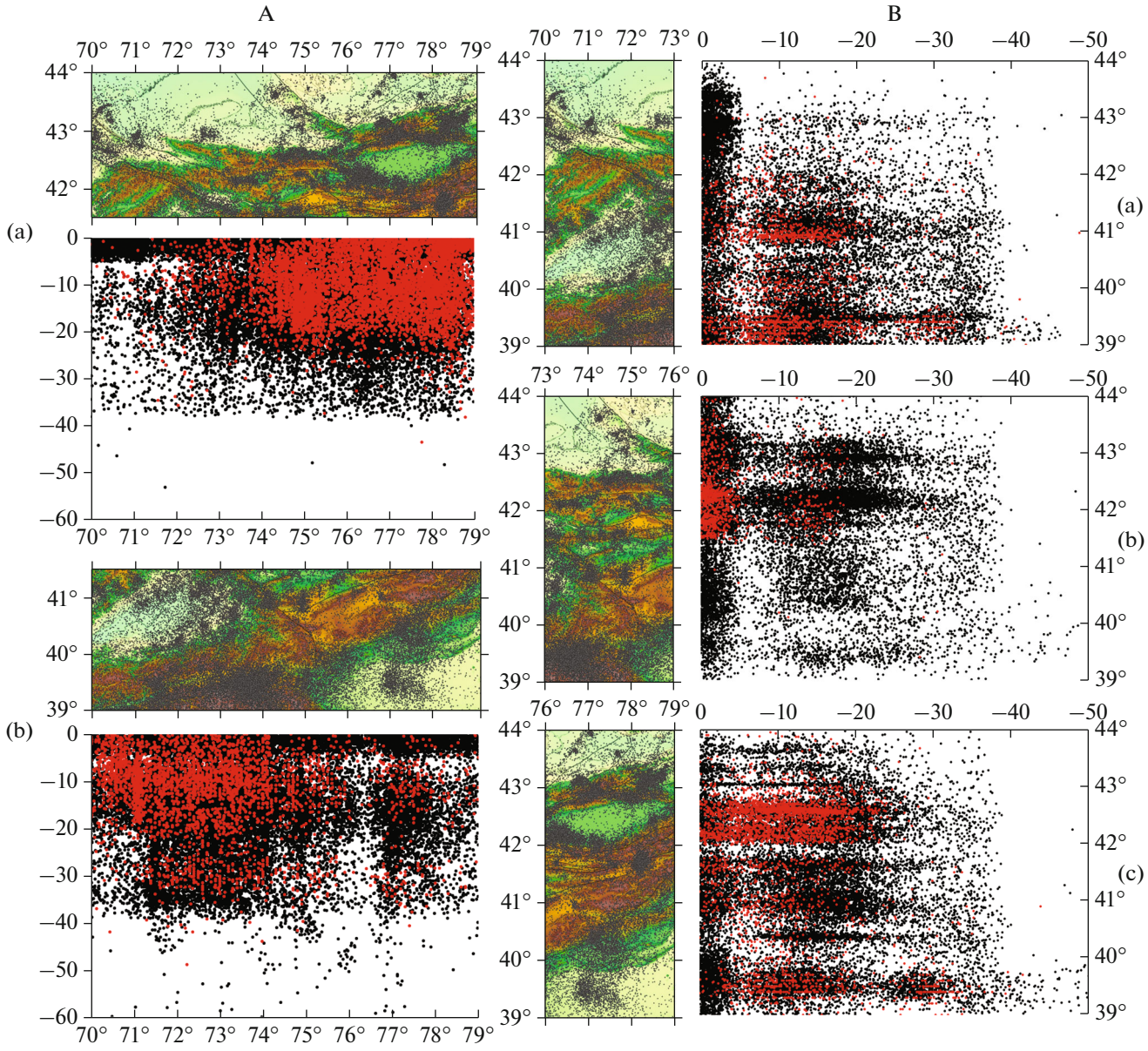

Fig. 4. The projections of earthquakes onto the vertical plane. (A) east–west cross section: (a) 41.5°–44° N (ISC has 28958 events and FM, 6424), (b) 39°–41.5° N (ISC has 27808 events and FM, 3115); (B) north–south cross section: (a) 70°–73° E (ISC has 16434 events and FM, 1898), (b) 73°–76° E (ISC has 21829 events and FM, 3524), (c) 76°–79° E (ISC has 18503 events and FM, 4117).

much smaller. The parameter is practically not determined in the Northern Tien Shan zone at depths over 25 km, because no earthquakes occur at these depths, except for the easternmost part of the Issyk Kul Basin. High levels of the parameter only remain along the zone where the Southern Tien Shan is adjacent to the Northern Pamirs and to Tarim.

Characteristics of the Principal Stress Axes

The catalog of focal mechanisms contains, along with hypocenter parameters, also characteristics of the principal stress axes: azimuth and plunge; these were used for statistical analysis to reveal some patterns in focal mechanism solutions. Statistical characteristics of the principal stress axes (azimuth and plunge) allow one to determine some patterns in deformation processes. Figure 7A shows diagrams of the azimuth distribution for compression and tension axes, as well as plots with the number of earthquakes versus the plunhe values for these axes.

The compression axes for most earthquakes in the area of study vary in direction from north–northwest to north–northeast, and the tension axes vary their

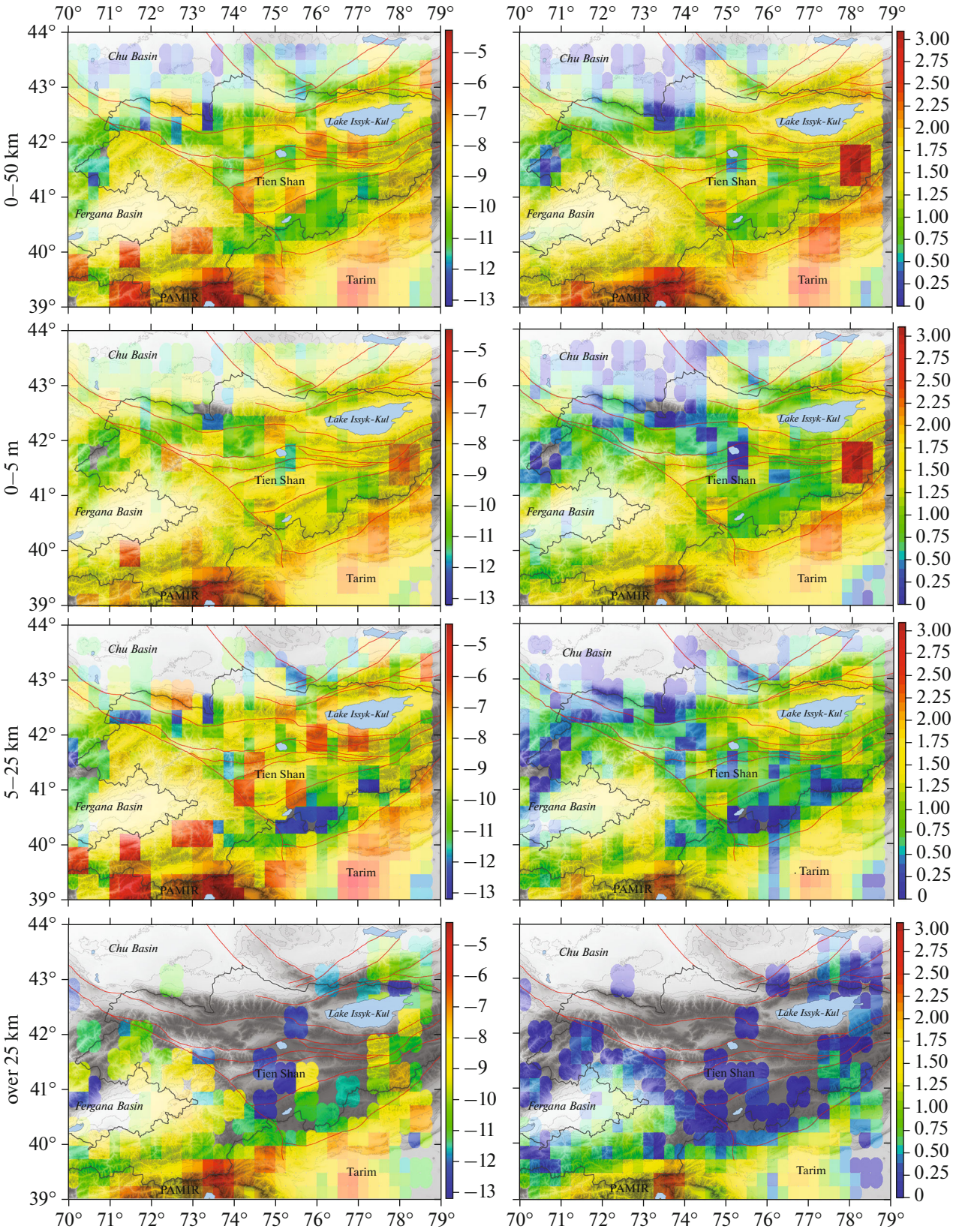

Fig. 5. The distribution of log STD intensity and of the number of earthquakes in the area of study for different depths based on data from the ISC catalog.

directions between northeast and east. A few of the tension axes also show different directions. The results obtained in this study are in good agreement with previous publications (Yunga, 1990; Kurskeev, 2004; Sycheva et al., 2005, 2008). More than a half (60%) of all compression axes have plunge values reaching 30° (near horizontal directions), while the tension axes have two equally important maxima, 0° and 50°–60°.

The entire area of study was subdivided into six areas (segments), with each including 3° longitude and 2.5° latitude. For each area we constructed diagrams showing the azimuth distribution for compression and tension axes (see Fig. 7B). One can clearly see a change in direction for the compression axes going from east to west, namely, from north to northwest.

The Average Mechanism and STD Regimes

As mentioned above, the calculation for maps of averaged source mechanisms was based on grid points at a step of 0.5°, while the averaged mechanisms in STD calculations were based on grid points at a step of 0.2° between the points, hence the configurations of the points for which we obtained the solutions differ between the two cases. The averaged mechanisms were found for points at which the coefficient κ (kappa, i.e., the intensity of the resulting matrix) exceeds that value from Table 4 (Yunga, 1990, pp. 88–89), where the mode and critical values of the parameter κ are presented corresponding to different cumulative probabilities and sample sizes. In this calculation, the contribution of an earthquake was given by a weight to be found from the relation $w = 0.07(M + 6)$, where M is the earthquake magnitude[1].

The maps of averaged mechanisms and STD maps were made for two depth ranges, 0–5 km and 5–25 km (Figs. 8, 9). There were few earthquakes at depths over 25 km in the catalog of focal mechanisms, thus placing a restriction on the study of deeper layers.

Averaged mechanisms of earthquake sources enable us to visualize both the statistics of focal mechanisms as a summary picture of projected P and T axes and the variation in deformation regime from point to point in the area of study. According to Fig. 8a, the data are the most complete for the Issyk Kul Basin and its circumference, for the eastern Kirgizsky mountain range, and for the junction zone between the Southern Tien Shan and the Northern Pamirs, as well as for the area along the Talas–Fergana fault (seismic zones). The shortening axes of average mechanisms have a northeastern direction west of the Talas–Fergana fault and a nearly north–south direction east of it. The reporting of seismicity for the northern part of the Tarim is the lowest, with the data indicating a northeastern direction for the shortening axes.

Figure 9a shows averaged mechanisms for the depth range 5–25 km. One must add the Fergana Basin to the list of areas with complete reporting as indicated for depths of 0–5 km. The directions of shortening axes at these depths are more to the north–northwest when west of the Talas–Fergana fault and toward north and northeast when east of the fault.

The STD map for the shallow layer (0–5 km) is shown in Fig. 8b. The orientation of the STD tensor at each grid element is marked by a symbol that indicates the direction of horizontal strain components and their fraction (part) in the total tensor. An absence of earthquakes in some areas of the shallow layer has limited the number of grid points for which solutions have been derived. As an example, there are practically no solutions for the junction zone between the Southern Tien Shan and Tarim. In the depth range under consideration we observe a diversity of STD regimes; this can be explained by fragmentation and blocky structure of the shallow crustal layer. In addition to the regimes (modes) shown in the right part of the classification scheme for STD regimes (see inset in Fig. 8b, the transitional regime from vertical shear to compression, horizontal compression, transpression, oblique shear, and horizontal shear), some areas in the region of study show modes from the left part (horizontal tension, the transitional regime from vertical shear to tension, and the transitional regime from tension to horizontal shear).

The following regimes are observed for the earthquake-generating layer (5–25 km) (see Fig. 9b): the transitional regime from vertical shear to compression (the west side of the Fergana valley, the junction zone between the Southern Tien Shan and the Northern Pamirs, the piedmont of the western Kirgizsky mountain range); horizontal compression (the east side of the Fergana Basin, the Chatkal Mountains, the Talas, Zailiisky, and Kungei Alatau mountain ranges); transpression (the southern Talas–Fergana fault, the eastern Kirgizsky mountain range, the Kochkor Basin, the Syndyk, Kyzart, and Terskei Alatau mountains, the eastern part of the junction zone between the Southern Tien Shan and the Tarim); horizontal shear regime (the southern Talas–Fergana fault, the Suusamyr Basin, and the central Kirgizsky mountain range, the Chu–Ili mountains).

An analysis of STD modes and the directions of shortening axes in different areas over the region of study for the earthquake-generating layer (5–25 km) is displayed in Table 5. The dark blue in the first column denotes the total deformation of horizontal shortening, light blue indicates the presence of horizontal shear regimes. The text color in the second column corresponds to that of STD regime according to the classification of STD regimes. The third column has the directions of shortening axes marked.

[1] Yunga, S.L., *A Study of Crustal Movements and Deformations in Central Tien Shan, the Kazakh Platform, and Altai; Developing a Program for Processing of Seismological Data, the Processing Carried out*, A research report, Obninsk, 2002. 41 p.

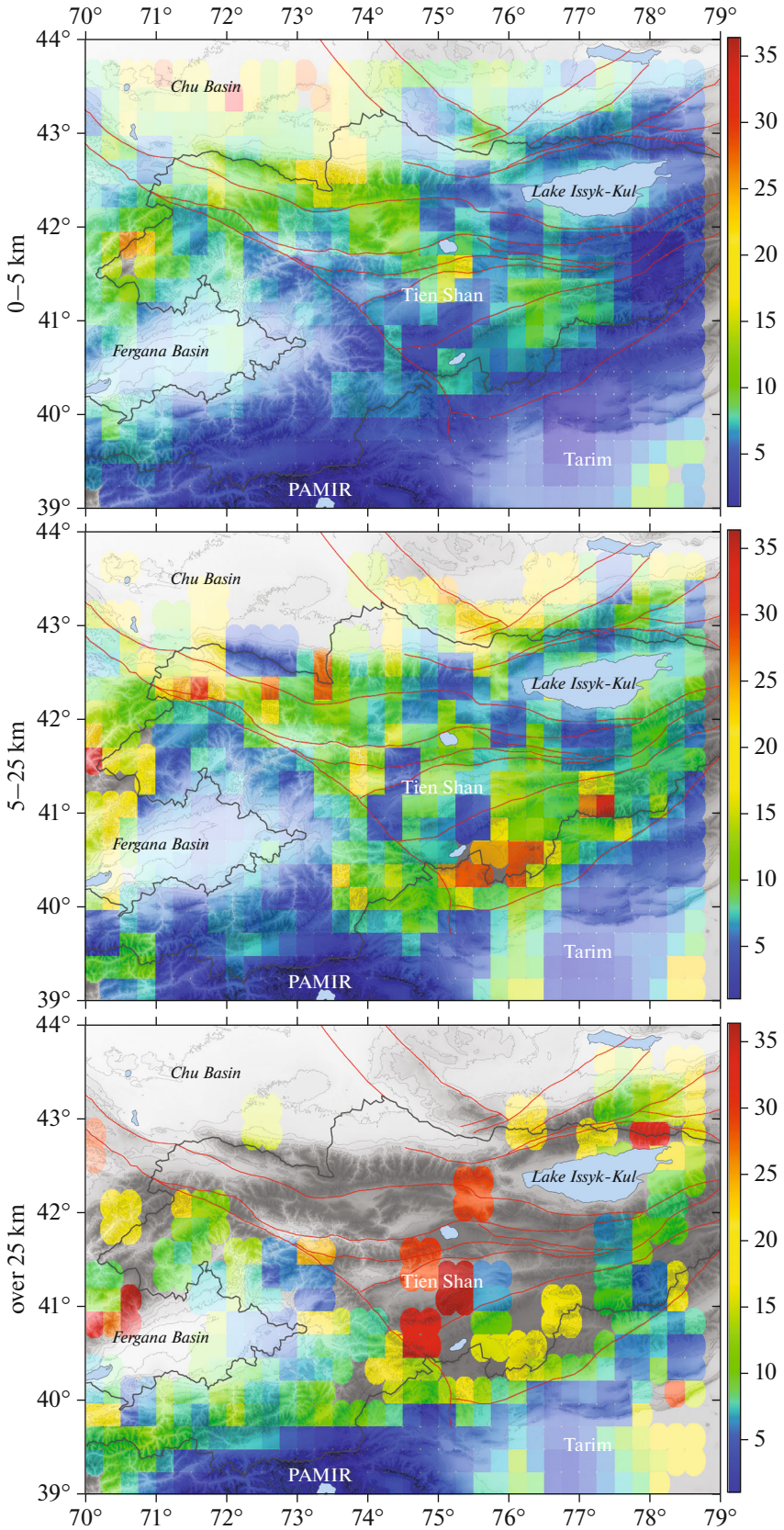

Fig. 6. The distribution of the concentration of earthquake-generating ruptures in the area of study for different depths based on data from the ISC catalog.

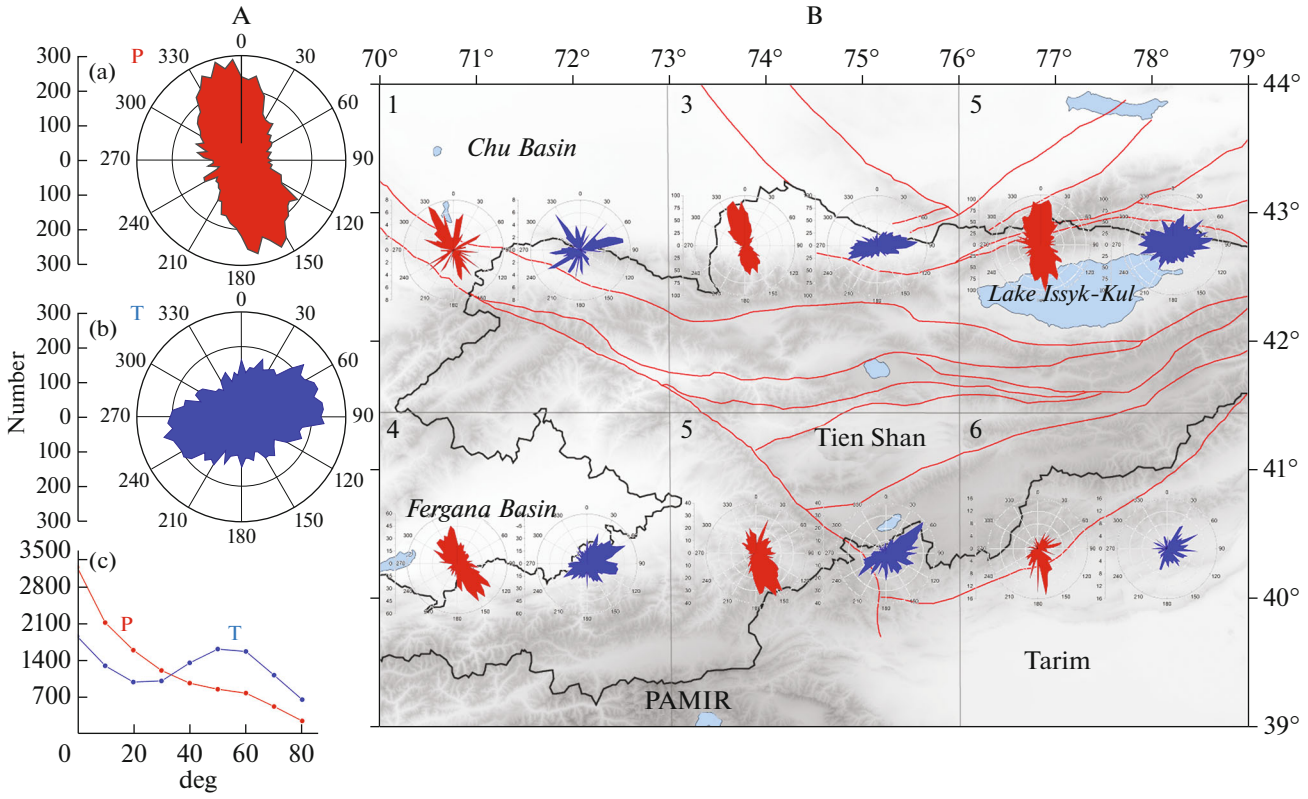

Fig. 7. Diagrams showing the distribution of azimuths for compression axes (a) and tension axes (b), and plots of the number of earthquakes versus plunge angles for these axes (c) for earthquakes from the FM catalog (A); diagrams showing the distribution of azimuths for compression and tension axes for different segments of the area of study: (1) 41.5°–44° N—70°–73° E; (2) 39°–41.5° N—70°–73° E; (3) 41.5°–44° N—73°–76° E; (4) 39°–41.5° N—73°–76° E; (5) 41.5°–44° N—76°–79° E; (6) 39°–41.5° N—76°–79° E (B).

An Analysis of STD Parameters

We examined the various STD parameters for the 5–25-km layer, which generated 7327 earthquakes present in the catalog of focal mechanisms, thus totaling 64% of all events.

The Lode–Nadai coefficient. The distribution of the Lode–Nadai coefficient is shown in Fig. 10A(a). The red color in this figure marks the regime of simple compression ($0.6 \le \mu_\varepsilon \le 1$), yellow indicates the regime of pure shear ($-0.2 \le \mu_\varepsilon \le 0.2$), the regime of simple tension is marked by blue ($-1 \le \mu_\varepsilon \le -0.6$), the dominance of simple compression (compression combined with shear) ($0.2 < \mu_\varepsilon < 0.6$) by red-yellow tints, and the dominance of simple tension (tension combined with shear) by green tints ($-0.6 < \mu_\varepsilon < -0.2$). According to the Legend (see Fig. 10A(a), at bottom), the regime of simple compression ($0.6 \le \mu_\varepsilon \le 1$) characterizes several areas. One of these includes the eastern Kirgizsky mountain range, the Kochkor Basin and its immediate circumference. The next includes the eastern Terskei Alatau. The junction zone between the Southern Tien Shan and the Northern Pamirs in its central and eastern parts is also characterized by the regime of simple compression. This list terminates in individual areas that are disposed in a fragmentary manner along the Talas–Fergana fault. The regime of simple shear occurs in the territory of the Chu, Issyk Kul, and Suusamyr basins, as well as in the Alai valley. The north side of the Fergana Basin is characterized by simple tension combined with shear ($-0.6 < \mu_\varepsilon < -0.2$).

The vertical component, which is not displayed visually in STD maps, has positive values everywhere over the area of study, except for the northern Chu Basin (see Fig. 10A(b)), which provides evidence of crustal uplifting nearly everywhere in the area of study.

Comparing the Crustal Deformation Results Based on Seismic and GPS Data

The distribution of the sum of horizontal components in the strain rate tensor (XX + YY, the maximum shortening rate) was derived from seismological data in the limits indicated in (Zubovich and Mukhamediev, 2010), with the distribution of maximum shortening rate being based on GPS observations for the most effective comparison between the results derived by the two methods (see Fig. 10B). One notes that the parameter of interest is inhomogeneous over the area of Tien Shan. Maximum shortening in the horizontal

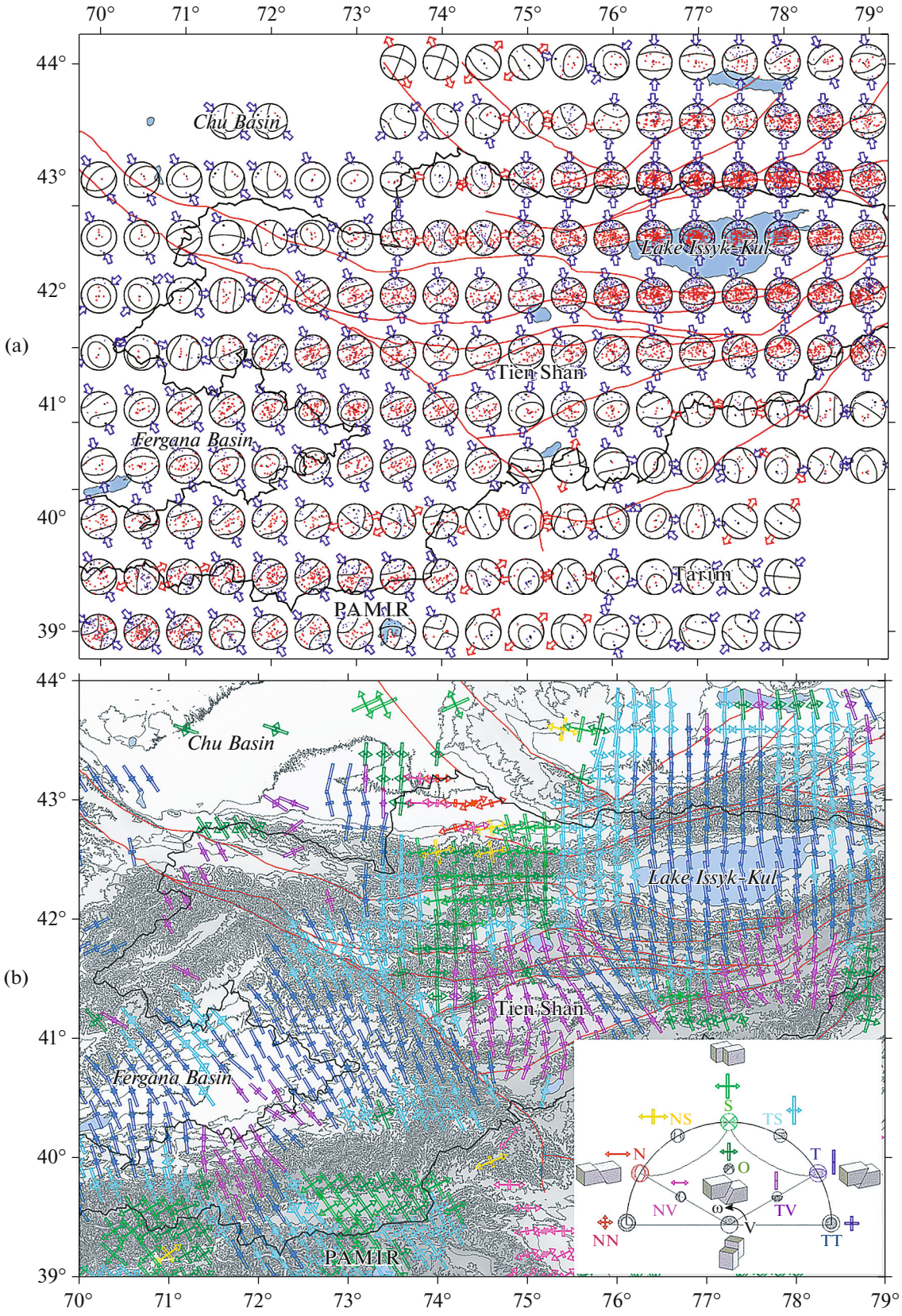

Fig. 8. Averaged source mechanisms (a) and a STD map (b) for depths of 0–5 km (3570 events). The color of a symbol denotes the pertinent deformation regime according to the classification shown in inset (Yunga, 1997). Red lines represent regional faults.

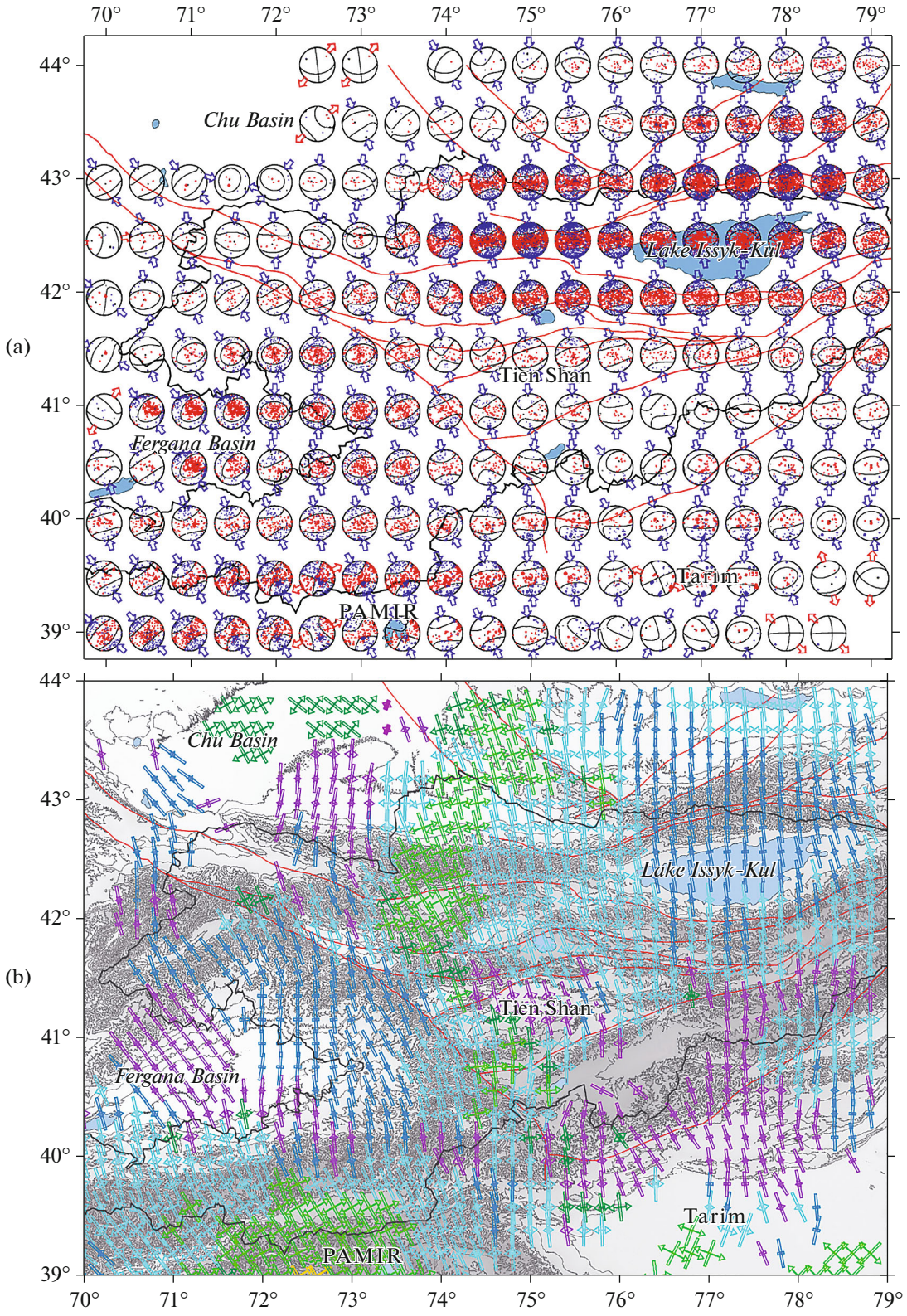

Fig. 9. Averaged source mechanisms (a) and a STD map (b) for depths of 5–25 km (7327 events). The color of a symbol denotes deformation regime according to the classification of STD regimes. Red lines represent regional faults.

Table 5. The STD regimes in the crust (5–25 km) for various areas in the region of study, and the directions of shortening axes

Area	STD regime (see inset in Fig. 8b)	Direction of shortening axes
Issyk Kul Basin and immediate surroundings	Compression, transpression	North, north-northwestern (*eastern part*)
Fergana Basin	Intermediate regime between vertical shear and horizontal compression, horizontal compression, transpression	Northwest (*north and west sides of basin*), north (*central part of basin*), north–northwestern (*east side of basin*)
Kirgizsky mountain range (Northern Tien Shan)	Transtional regime between vertical shear and horizontal compression, horizontal compression (western part), horizontal shear (central part), transpression (eastern part)	North (western part), north-northwestern (central part), northern (eastern part)
Talas-Fergana fault	Horizontal shear and transpression (southern part) horizontal compression (central part), transpression and oblique shear (northern part)	North–northwestern
Junction of Southern Tien Shan and Tarim	Transitional regime between vertical shear and horizontal compression, horizontal compression	North–northwestern (*western part*) and northern and north–northeastern (*eastern part*)
Junction of Southern Tien Shan and Pamirs	Horizontal compression , (easternmost part), transpression (eastern and western parts), horizontal shear (central part)	North (*easternmost part*), north–northwestern (*eastern and central parts*), northwestern (*western part*)

plane is characteristic for the sides of the Issyk Kul Basin (Kungei and Terskei Alatau, as well as the Zailisky mountain range), for the northeast sides of the Fergana Basin (the Baubashata, East Alai, and Fergana mountain ranges), for the western Chu Basin, as well as for the junction zone between the Southern Tien Shan and Tarim.

Figure 10B(b) presents the map of maximum shortening rate from (Zubovich and Mukhamediev, 2010), who note that the Kazakh Shield north of Tien Shan is nearly free of shortening, while Tien Shan itself shows a rather inhomogeneous E2 field, with stable areas being adjacent to zones of higher shortening rates. Considerable shortening deformation E2 is observed near Lake Issyk Kul where eastern and southwestern zones are clearly seen upon the background of a moderate nearly north–south shortening. Another example of a zone characterized by high shortening rates is the Naryn Basin. One also notes two areas of moderate negative values of E2 in northern Tien Shan. The one lies near Bishkek and is obviously related to the movement on the Issyk–Ata fault.

Comparison of the distribution of maximum shortening based on seismic (see Fig. 10B(a)) and GPS observations (see Fig. 10B(b)) showed fairly good consistency between the results. One also notes that areas that were identified to have maximum shortening based on both seismic and GPS data are characterized

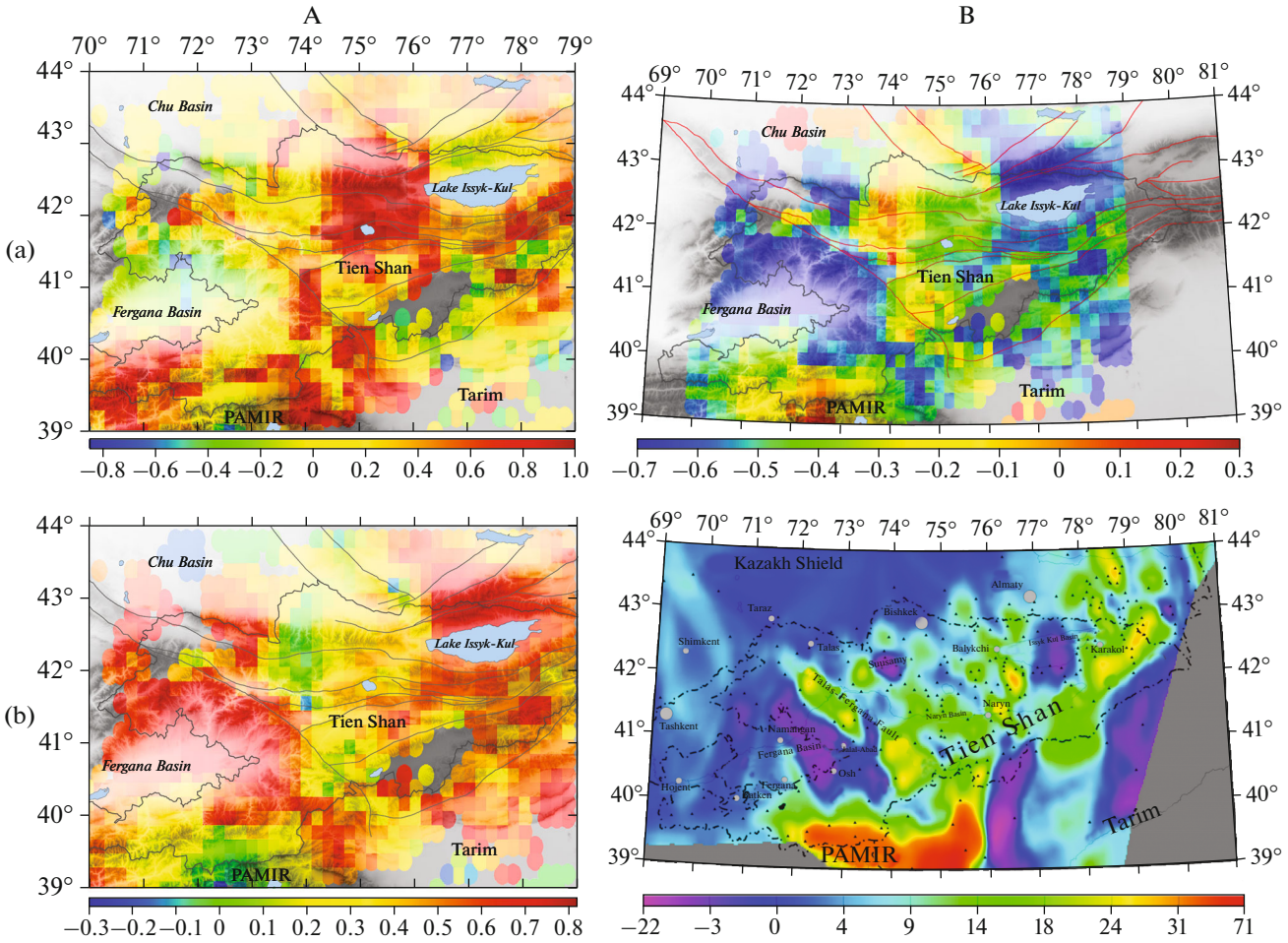

Fig. 10. The distribution of the Lode–Nadai parameter (a) and of the vertical component ZZ (b) of the strain rate tensor for the earthquake-generating layer, 5–25 km (A); the distribution of area-change deformation (XX + YY) (the sum of horizontal longitudinal components in the strain rate tensor) based on seismological data for the earthquake-generating layer, 5–25 km. The unit of measurement is 10^{-9} year^{-1} (a). A map of maximum shortening rate E2 (after Zubovich and Mukhamediev (2010)) (b). The dash–dotted lines mark state borders (B).

by maximum positive values of the vertical component (see Fig. 10A(b)).

The directions of shortening and lengthening axes as obtained from seismic and GPS observations were compared in (Kostyuk et al., 2010; Sycheva and Mansurov, 2016; Sycheva and Mansurov, 2017; Sycheva and Mansurov, 2020). These studies were concerned with Northern Tien Shan, Central Tien Shan, and with the Pamirs and adjacent areas. It was shown that the directions of shortening axes as determined by the two methods, not only are well consistent among themselves, but can also complement each other.

Figure 11 presents the distribution of the crustal strain rate tensor based on GPS data from (Mansurov, 2017) along with the distribution of the generalized plane part of the STD direction tensor for the depth range 5–25 km as derived in the present study. In contrast to STD where the intensity of seismotectonic deformation is found by summing seismic moments, resulting in a distribution of that field, the deformation intensity based on the GPS method is expressed in the lengths of shortening and lengthening axes. Even though the seismic data are used for the depth range 5–25 km, the overall visual inspection reveals a good consistency between the directions and the type of horizontal deformation as derived by the two methods. This consistency may provide evidence that GPS data reflect deformation, not only of the shallow layer, but also of the deformed crust as a whole.

We compared numerically the directions of shortening axes based on GPS and STD data by considering segments where the two fields are present (rectangles, see Fig. 11). For these segments we found the mean azimuths of shortening axes based on GPS and STD data, as well as determining, at each grid point, the difference between the azimuths of shortening axes, and calculating the mean difference for the segment. The results of this calculation are presented in Table 6,

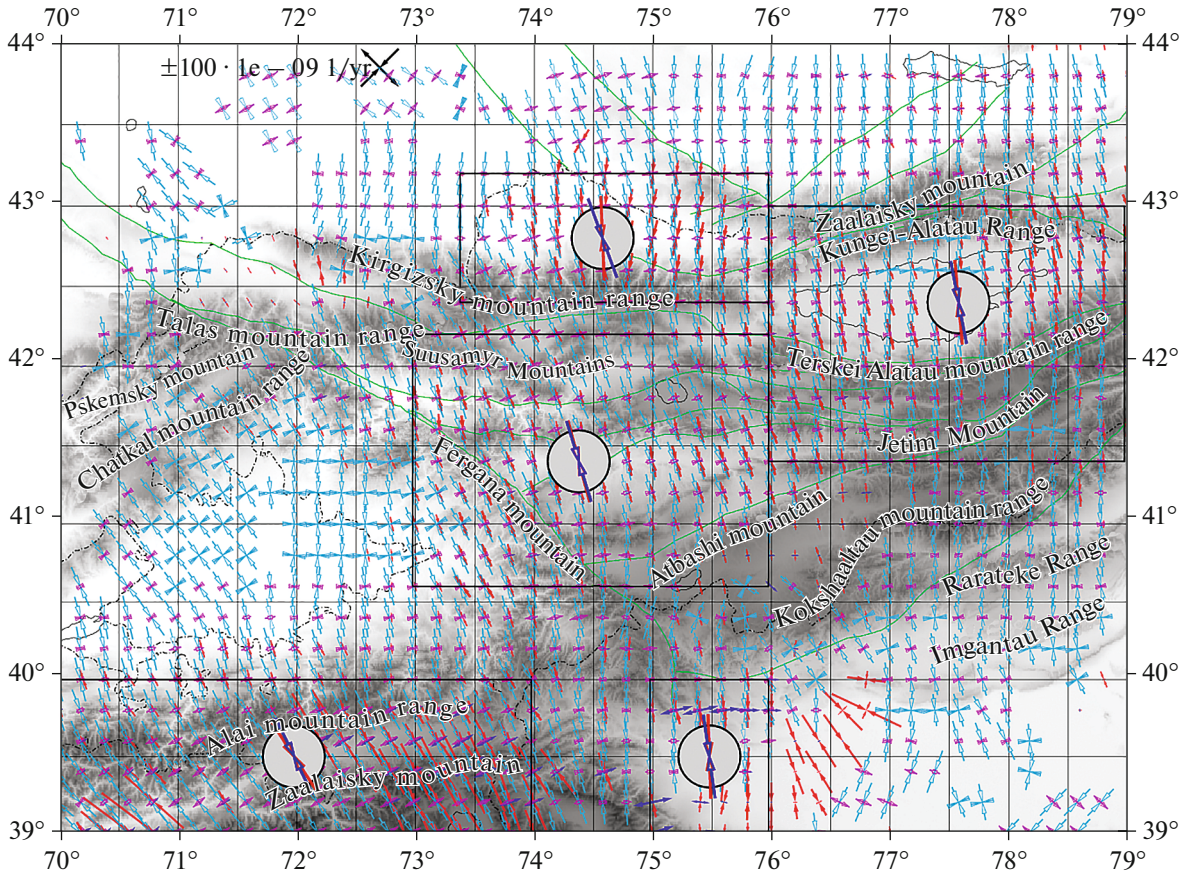

Fig. 11. The results of STD calculation for depths of 5–25 km (this differs from Fig. 9b in color only; light blue denotes shortening axes and raspberry color denotes lengthening axes) superimposed on the map of present-day crustal strain rate tensor based on GPS observations (Mansurov, 2017). Red arrows show the direction and intensity of shortening, blue arrows show the direction and intensity of lengthening based on GPS observations according to the scale in the top right corner. Rectangles mark the segments from Table 6.

while Fig. 11 displays averaged directions of shortening axes for the segment (those marked red are based on GPS data, with blue marking STD observations). The lowest difference between the mean values is 0° (the segment in the right part of the map, see Fig. 11), the highest is 11° (the top segment, see Fig. 11). The difference between the directions of shortening axes may range between 0.1° and 25° at some grid points, with the averaged value of the deviation varying between 6.5° and 11.1°. These results can be related to the peculiar properties of each method, as well as to the quality of the data used. As an example, the maximum difference in the directions of shortening axes is characteristic for the northern piedmont of the Kirgizsky mountain range (the top segment, see Fig. 11). The discrepancy can be explained by the fact that the

Table 6. Segment coordinates, number of grid points, mean value of directions of shortening axes based on GPS and STD data for a segment and the difference between these, minimum, maximum, and mean difference of point-by-point comparison

No.	φ_1,° N	φ_2,° N	λ_1,° E	λ_2,°E	N	Mean direction of compression axis based on data, °			Value of |GPS-STD|, ° at grid point		
						GPS	STD	|GPS-STD|	Min.	Max.	Mean
1	42.4	43.2	73.4	76.0	23	358	347	11	1.13	20.43	11.1
2	41.4	43.0	76.0	79.0	43	354	354	0	0.09	16.73	6.5
3	40.6	42.2	73.0	76.0	37	345	343	2	0.37	25.34	6.96
4	39.0	40.0	75.0	76.0	11	358	354	2	0.24	20.72	6.83
5	39.0	40.0	70.0	74.0	80	330	334	4	0.02	22.84	6.78

STD calculation for the area mainly relied on the catalog of focal mechanisms based on the KNET network data with 10 seismic stations, with most mechanisms being based on 7–8 P-wave first motions. As well, the catalog mostly contains low magnitude events, which reflect local deformation regimes, while large events that are mostly used to find regional directions of compression axes have not occurred in the area for the period of interest.

Overall, even though there are appreciable differences in the data for some grid points, the averaged directions of shortening axes based on GPS and STD data are in good agreement (see Fig. 11).

There are grid points in Fig. 11 where the data came from a single one of the two methods. As an example, it was only GPS data which were used to find the directions of shortening and lengthening axes at several grid points in the northwestern Tarim, while on the other hand, it was only by the STD method that the deformation regime was determined for the eastern part of the junction zone between the Southern Tien Shan and Tarim, as well as at the circumference of the Fergana Basin. The results of the numerical comparison presented in Table 6 and in Fig. 11 lead us to conclude that the lack of data on deformation regime for one of the methods can to a certain degree of confidence be supplemented with data of the other method.

CONCLUSIONS

We used seismic data (the ISC catalog with over 84000 events for 1902–2019) and data on focal mechanisms of earthquakes (11376 events for 1946 to 2020) to examine the state of crustal stress and strain for Western and Central Tien Shan. Integral projections onto the vertical plane were used to find that earthquakes in the area of study occurred at depths of 0–50 km. The 5–25-km layer shows the highest seismic activity. Some of the earthquakes also occurred in the shallow layer (0–5 km) and at depths greater than 25km (mostly in the south of the study area). Seismic activity (number of earthquakes), STD intensity, and the concentration of earthquake-generating ruptures were calculated for three depth ranges, 0–5, 5–25, and over 25 km. At all of these depths, the highest STD intensity and the largest numbers of earthquakes occurred in the zone where the Southern Tien Shan is adjacent to the Northern Pamirs and Tarim. Down to 25 km depth in the north of the study area, high values of STD intensity are observed in the western Terskey Alatau and in the eastern Kirgizsky mountain range, high seismic activity occurred in the Northern Tien Shan earthquake-generating zone. At depths of 0–5 km, high levels of the concentration of earthquake-generating ruptures is characteristic for the entire area of study, except for its northwest. At depths of 5–25 km, the areas having high levels of crack concentration are smaller, while at depths greater than 25 km a high level of that parameter only remains along the zone where the Southern Tien Shan is adjacent to the Northern Pamirs and Tarim.

We estimated parameters of the state of stress and strain for the area of study using the STD method. The catalog of focal mechanisms was used to make diagrams showing the directions of the principal stress axes. For most of the earthquakes, the compression axis changes direction from northwestern when west of the Talas–Fergana fault to north–south when east of the fault. Most of the axes are nearly horizontal. Maps of averaged focal mechanisms and STD maps were made for depths of 0–5 km and 5–25 km. The shallow layer shows a great diversity of STD regimes, including as they do, not only compression combined with various levels of strike slip components, but also tension combined with various fractions of the shear component. The earthquake-generating layer (5–25 km) shows compression regimes combined with various levels of the shear component, viz., the transitional regime from vertical shear to compression, horizontal compression, transpression, and horizontal shear. The construction of the distribution of the Lode–Nadai coefficient showed that simple compression involves an area that includes the eastern Kirgizsky mountain range, the Kochkor Basin and its immediate surroundings, the eastern Terskei Alatau, as well as the junction zone between the Southern Tien Shan and the Northern Pamirs in its central and eastern parts, and fragmentary areas along the Talas–Fergana fault. Simple shear is observed in most basins and in the Alai valley, while the Fergana Basin is characterized by tension combined with shear.

Maximum shortening affects the northern circumference of the Issyk Kul Basin (Kungei Alatau and Zailiisky mountain range); the northwest side of the Fergana Basin (the Baubashata, East Alai, and Fergana mountain ranges), and the eastern part of the junction zone between the Southern Tien Shan and Tarim. The entire area of study, except for the northern Chu Basin, experiences uplifting (the ZZ component): the maximum uplifting occurs in the same areas where the maximum change in area has been identified.

The deformation models for the area of study using the STD method and GPS data were compared to show good agreement: the directions of the principal axes in the horizontal part of the tensor are either identical or similar, the deformation regimes over most of the area are identical as well.

ACKNOWLEDGMENTS

I am grateful to Artur Mansurov who lent me use his results from the calculation of present-day crustal strain rate tensor based on GPS observations.

FUNDING

This work was supported in part by a state assignment at the Research Station of the Russian Academy of Sciences,

Bishkek (research topics AAAA-A19-119020190064-9 and AAAA-A19-119020190066-3).

REFERENCES

Abdrakhmatov, K.E., Wildon, R., Thompson, S., et al., The origin, direction, and rate of present-day compression in central Tien Shan, Kirgizia, *Geol. Geofiz.,* 2001, vol. 42, no. 10, pp. 1585–1610.

Burtman, V.S., *Tyan-Shan i Vysokaya Aziya* (Tien Shan and High Asia), Moscow: GEOS, 2012.

Chediya, O.K., *Morfostruktury i noveishii tektogenez Tyan-Shanya* (The Morphostructures and Neotectonic Tectogenesis of Tien Shan), Frunze: Ilim, 1986.

International Seismological Centre, On-line Bulletin, 2019. Available from: http://www.isc.ac.uk (last accessed 10.06.2020).

Kalmetieva, Z.A., Kostyuk, A.D., and Sycheva, N.A., On relationships between landslides and earthquakes, *Izv. NAN KR,* Bishkek: Ilim, 2010, no. 4, pp. 22–29.

Kostyuk, A.D., Sycheva, N.A., Yunga, S.L., et al., Crustal; deformation in Tien Shan based on earthquake mechanisms and space geodesy, *Fizika Zemli,* 2010, no. 3, pp. 52–65.

Krestnikov, V.N., Shishkin, E.I., Shtange, D.V., and Yunga, S.L., The state of stress in the crust of Central and Northern Tien Shan, *Izv. AN SSSR, Fizika Zemli,* 1987, no. 3, pp. 13–30.

Kuchai, O.A. and Bushenkova, N.A., Focal mechanisms of Central Tien Shan, *Fiz. Mezomekh.,* 2009, vol. 12, no. 1, pp. 17–24.

Kurskeev, A.K., *Zemletryaseniya i seismicheskaya bezopasnost Kazakhstana* (Earthquakes and the Seismic Safety of Kazakhstan), Almaty: Evero, 2004.

Kuzikov, S.I. and Mukhamediev, Sh.A., The structure of the present-day crustal movement rates in the area of the Central Asia GPS network, *Fizika Zemli,* 2010, no. 7, pp. 33–51.

Lukk, A.A., Shevchenko, V.I., and Leonova, V.G., Autonomous geodynamics of the Pamir–Tien Shan junction zone from seismology data, *Physics of the Solid Earth,* 2015, vol. 51(6), pp. 859–877.

Lukk, A.A. and Shevchenko, V.I., Seismicity, tectonics, and GPS geodynamics of the Caucasus, *Izv., Physics of the Solid Earth,* 2019, vol. 55(4), pp. 626–648.

Lukk, A.A. and Yunga, S.L., The seismotectonic deformation in the Garm area, *Izv. AN SSSR, Fizika Zemli,* 1979, no. 10, pp. 24–43.

Makarov, V.I., *Noveishaya tektonicheskaya struktura Tsentralnogo Tyan-Shanya* (The Neotectonic Structure of Central Tien Shan), Moscow: Nauka, 1977.

Mamyrov, E., Omuraliev, M., and Usupaev, Sh.E., *Otsenka veroyatnoi seismicheskoi opasnosti territorii Kyrgyzskoi Respubliki I prigranichnykh raionov stran Tsentralnoi Azii na period 2002–2005 gg.* (Assessment of Probable Earthquake Hazard to the Territory of the Kyrgyz Republic and Adjacent Areas of Countries in Central Asia for the Period 2002–2005), Bishkek, 2002.

Mansurov, A.N., A continuum model of present-day crustal deformation in the Pamir-Tien Shan region constrained by GPS data, *Russian Geology and Geophysics,* 2017, vol. 58, no. 7, pp. 787–802. https://doi.org/10.1016/j.rgg.2017.06.002

Midi, B. Dzh. and Khager, B.Kh., The present-day distribution of deformation in western Tien Shan using block models based on geodetic data, *Geol. Geofiz.,* 2001, vol. 42, no. 10, pp. 1622–1633.

Rebetsky, Yu.L., *Tektonicheskie napryazheniya i prochnost' prirodnykh massivov* (Tectonic Stresses and the Strength of Natural Rock Massifs), Moscow: Akademkniga, 2007.

Rebetsky, Yu.L. and Alekseev, R.S., The field of recent tectonic stresses in Central and South-Eastern *Geodyn. Tectonophys., Asia*, 2014, vol. 5(1), pp. 257–290. https://doi.org/10.5800/GT-2014-5-1-0127

Rebetsky, Yu. L., Sycheva, N.A., Kuchay, O.A., and Tatevossian, R.E., Development of inversion methods on fault slip data. Stress state in orogenes of the central Asia, *Tectonophysics,* 2012, vol. 581, pp. 114–131. https://doi.org/10.1016/j.tecto.2012.09.027

Rebetsky, Yu.L., Sycheva, N.A., Sychev, V.N., et al., Crustal stresses in Northern Tien Shan based on data from the KNET network, *Geol. Geofiz.,* 2016, vol. 57, no. 3, pp. 496–520.

Reigber, C., Michel, G.W., Galas, R., et al., New space geodetic constraints on the distribution of deformation in central Asia, *Earth Planet. Sci. Lett.,* 2001, vol. 191(1–2), pp. 157–165. https://doi.org/10.1016/S0012-821X(01)00414-9

Riznichenko, Yu.V., The source dimensions of the crustal earthquakes and the seismic moment, in *Issledovaniya po fizike zemletryasenii* (Studies in Earthquake Physics), Moscow: Nauka, 1976, pp. 9–27.

Riznichenko, Yu.V., *Problemy seismologii* (Problems in Seismology), Moscow: Nauka, 1985.

Sadybakasov, I., *Neotektonika Vysokoi Azii* (The Neotectonics of High Asia), Moscow: Nauka, 1990.

Search form, Global CMT Catalog Search. URL: https://www.globalcmt.org/CMTsearch.html (date of request: June 12, 2020).

Shults, S.S., *Analiz noveishei tektoniki i relief Tyan-Shanya* (An Analysis of Neotectonics and Relief of Tien Shan), Moscow: Geografgiz, 1948.

Sobolev, G.A. and Zav'yalov, A.D., On the concentration criterion of earthquake-generating ruptures, *Dokl. AN SSSR,* 1980, vol. 252, no. 1, pp. 69–71.

Sovremennaya geodinamika oblastei vnutrikontinentalnogo kollizionnogo goroobrazovaniya (Tsentralnaya Aziya) (Present-Day Geodynamics of Areas of Intracontinental Collisional Orogenesis: Central Asia), Moscow: Nauchnyi Mir, 2005.

Sycheva, N.A., Seismic moment tensor and dynamic parameters of earthquakes in the Central Tien Shan, *Geosistemy perekhodnykh zon* (Geosystems of Transition Zones), 2020, vol. 4, no. 2, pp. 192–209. (In Engl.). https://doi.org/10.30730/gtrz.2020.4.2.178-191.192-209

Sycheva, N.A. and Mansurov, A.N., Comparing the estimates of crustal deformation for northern and central Tien Shan based on GPS and seismic data, *Vestnik KRSU,* 2016, vol. 16, no. 1, pp. 178–182.

Sycheva, N.A. and Mansurov, A.N., Comparing the estimates of crustal deformation at the Bishkek Geody-

namic Test Site based on seismological and GPS data, *Geodin. Tektonof.,* 2017, vol. 8, no. 4, pp. 809–825.

Sycheva, N.A. and Mansurov, A.N., Seismotectonic deformation of the lithosphere in the Pamir and adjacent territories, *Geodyn. Tectonophys.,* 2020, vol. 11(4), pp. 785–805. https://doi.org/10.5800/GT-2020-11-4-0507

Sycheva, N.A., Yunga, S.L., Bogomolov, L.M., et al., Crustal seismotectonic deformations in the Issyk Kul zone and in the Kazakh Tien Shan, in *Aktivnyi geofizicheskii monitoring litosfery Zemli* (Active Geophysical Monitoring of the Earth's Lithosphere), Novosibirsk, 2005, pp. 344–350.

Sycheva, N.A., Yunga, S.L., Bogomolov, L.M., and Mukhamadeeva, V.A., Crustal seismotectonic deformations in northern Tien Shan: Determinations of earthquake source mechanisms based on data from the KNET digital seismic network, *Fizika Zemli,* 2005a, no. 11, pp. 62–78.

Sycheva, N.A., Bogomolov, L.M., Yunga, S.L., and Makarov, V.I., Seismotectonic deformations and the neotectonics of Tien Shan, *Fizika Zemli,* 2008, no. 5, pp. 3–15.

Trifonov, V.G., Soboleva, O.V., Trifonov, R.V., and Vostrikov, G.A., *Sovremennaya geodinamika Alpiisko-Gimalaiskogo kollizionnogo poyasa* (The Present-Day Geodynamics of the Alpine–Himalayan Collisional Belt), Moscow: GEOS, 2002.

Trofimov, A.K., Udalov, N.F., Utkina, N.G., et al., *Geologiya kainozoya Chuiskoi vpadiny i ee gornogo obramleniya* (The Cenozoic Geology of the Chu Basin and Its Mountainous Circumference), Leningrad: Nauka, 1976.

Vinnik, L., Reigber, C., Aleshin, I., et al., Receiver function tomography of the central Tien Shan, *Earth Planet. Sci. Lett.,* 2004, vol. 225(1–2), pp. 131–146. doi.org/ https://doi.org/10.1016/j.epsl.2004.05.039

Yudakhin, F.N., *Geofizicheskie polya, glubinnoe stroenie i seismichnost Tyan-Shanya* (Geophysical Fields, Deep Structure, and Seismicity in Tien Shan), Frunze: Ilim, 1983.

Yudakhin, F.N., Chediya, O.K., Sabitova, T.M., et al., *Sovremennaya geodinamika litosfery Tyan-Shanya* (The Present-Day Geodynamics of the Tien Shan Lithosphere), Moscow: Nauka, 1991.

Yunga, S.L., *Metody i rezul'taty izucheniya seismotektonicheskikh deformatsii* (Methods for and Results from Studies of Seismotectonic Deformation), Moscow: Nauka, 1990.

Yunga, S.L., On the classification of seismic moment tensors based on their isometric imaging onto a sphere, *Dokl. Akad. Nauk,* 1997, vol. 352, no. 2, pp. 253–255.

Zav'yalov, A.D., *Srednesrochnyi prognoz zemletryasenii* (Intermediate-Term Earthquake Prediction), Moscow: Nauka, 2006.

Zubovich, A.V. and Mukhamediev, Sh.A., A method of superimposed triangulations for calculation of velocity gradient of horizontal movements: application to the Central Asian GPS network, *Geodyn. Tectonophys.*, 2010, vol. 1, no. 2, pp. 169–185.

Zubovich, A.V., Trapeznikov, Yu.A., Bragin, V.D., et al., The deformation field, deep crustal structure, and the spatial distribution of seismicity in Tien Shan, *Geol. Geofiz.,* 2001, vol. 42, no. 10, pp. 1634–1640.

Zubovich, A.V., Beisenbaev, R.T., Van Syaochin, et al., The present-day kinematics of the Tarim–Tien-Shan–Altai region in Central Asia: GPS measurements, *Fizika Zemli,* 2004, no. 9, pp. 31–40.

Zubovich, A.V., Wang, X., Scherba, Y.G., et al., GPS velocity field for the Tien Shan and surrounding regions, *Tectonics,* 2010, 29(6), TC6014. https://doi.org/10.1029/2010TC002772

Translated by A. Petrosyan